ACS APPLIED MATERIALS & INTERFACES

Research Article

www.acsami.org

Bioelectrochemistry of Heme Peptide at Seamless Three-Dimensional Carbon Nanotubes/Graphene Hybrid Films for Highly Sensitive Electrochemical Biosensing

Kikuo Komori,*[,†,‡] Trupti Terse-Thakoor,[§] and Ashok Mulchandani*[,‡]

[†]Institute of Industrial Science, University of Tokyo, Komaba, Meguro-ku, Tokyo 153-8505, Japan

[‡]Department of Chemical and Environmental Engineering, University of California, Riverside, California 92521, United States

[§]Department of Bioengineering, University of California, Riverside, California 92521, United States

Supporting Information

ABSTRACT: A seamless three-dimensional hybrid film consisting of carbon nanotubes grown at the graphene surface (CNTs/G) is a promising material for the application to highly sensitive enzyme-based electrochemical biosensors. The CNTs/G film was used as a conductive nanoscaffold for enzymes. The heme peptide (HP) was immobilized on the surface of the CNTs/G film for amperometric sensing of H_2O_2. Compared with flat graphene electrodes modified with HP, the catalytic current for H_2O_2 reduction at the HP-modified CNTs/G electrode increased due to the increase in the surface coverage of HP. In addition, microvoids in the CNTs/G film contributed to diffusion of H_2O_2 to modified HP, resulting in the enhancement of the catalytic cathodic currents. The kinetics of the direct electron transfer from the CNTs/G electrode to compound I and II of modified HP was also analyzed.

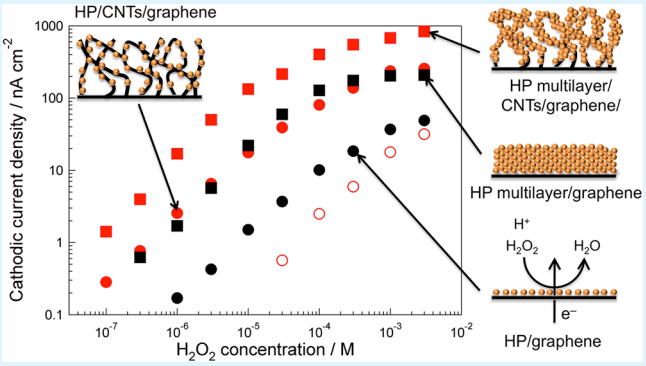

KEYWORDS: *three-dimensional film, carbon nanotubes-grown graphene, amperometric biosensor, heme peptide, H_2O_2 sensing*

INTRODUCTION

Nanomaterials based on sp^2 carbon, such as graphene and carbon nanotubes (CNTs), are one of the promising materials for the development of batteries, fuel cells, capacitors, electronics, and sensors, because of their high electrical conductivity, high specific surface area, and good chemical stability.[1−3] In particular, graphene and CNTs have attracted attention for the development of enzyme-based electrochemical biosensors, because of their ability to achieve direct electrochemical communication with redox enzymes,[4−7] which is otherwise difficult, because of the thick insulating polypeptide layer covering the active site. However, such superior properties emerge only in the planar direction for graphene or one direction for CNTs, because of their two- or one-dimensional structures, respectively. In addition, graphene and CNTs are widely used after their coating on a substrate, such as electrodes, but contact resistance among those sp^2 carbon-based materials is significant.

To overcome this limitation, seamless three-dimensional (3D) sp^2 carbon-based nanomaterials, such as foam-like graphene[8,9] and carbon nanotubes-grown graphene (CNTs/G) hybrid materials,[10,11] have recently been synthesized. Because of the seamless structure, these 3D carbon nanomaterials enable charge carriers to move in all three dimensions, without significant contact resistance. Furthermore, the 3D carbon nanomaterials also enable the enhancement of the total surface area per unit planar/footprint area on the substrate. Hence, it is expected to improve the sensitivity and/or expand the dynamic range, because of the increase in the amount of enzymes per unit area. For the development of biosensors, compared with the foamlike graphene, the CNTs/G film is particularly a preferred structure to attach on the substrate, because its backside is a flat surface. For instance, the CNTs/G film is expected to develop flexible and wearable biosensors for physiological monitoring. However, the electron transfer reaction at the interface of the CNTs/G film is not yet well elucidated.

Toward the development of highly sensitive enzyme-based electrochemical biosensors, there is a need for the elucidation of the electron transfer between the CNTs/G film and enzymes. In addition, the 3D structure-based microvoid effects on the sensitivity and/or dynamic range for an analyte also must be assessed. In the present work, we constructed a heme undecapeptide (HP)-modified CNTs/G film-coated (HP/CNTs/G) glassy carbon electrode and studied the kinetics of electron transfer from the CNTs/G film to HP, which has a

Received: November 17, 2014
Accepted: January 27, 2015
Published: February 6, 2015

DOI: 10.1021/am508032p
ACS Appl. Mater. Interfaces 2015, 7, 3647−3654

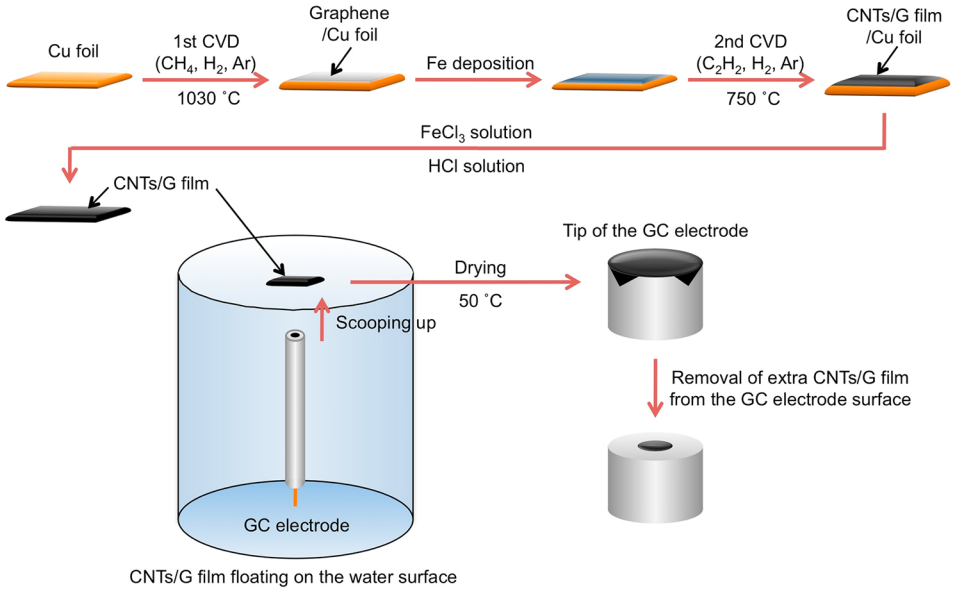

Figure 1. Schematic illustration of the preparation of CNTs/G electrode.

similar structure to the active center of peroxidase and has been used for H_2O_2 sensing.[12−14] By comparing with catalytic reduction currents of H_2O_2 at HP-modified graphene-coated (HP/G) electrodes, we showed advantages of the HP/CNTs/G electrode in the sensitive detection of H_2O_2. Furthermore, since the active center of HP is not fully covered with the insulating polypeptide and electrochemical responses for H_2O_2 at HP multilayer-modified electrode enhanced through the electron self-exchange among HP molecules. The microvoid effect at the HP multilayer-modified CNTs/G (HP-ML/CNTs/G) electrode on diffusion of H_2O_2 was also examined from the catalytic currents of H_2O_2 reduction in comparison with the case in the HP multilayer-modified graphene (HP-ML/G) electrode.

EXPERIMENTAL SECTION

Preparation of CNTs/G Hybrid Films. CNTs/G hybrid films were prepared by a two-step process (see Figure 1). First, graphene film was grown on the surface of a copper (Cu) foil (~6.5 cm^2 and 25 μm thick) via chemical vapor deposition (CVD). The Cu foil, which is a catalyst and substrate for graphene growth, was placed inside a quartz tube (ca. 3 cm in inner diameter and ca. 75 cm long) and annealed at 1030 °C under flowing Ar (190 sccm) and H_2 (10 sccm) at atmospheric pressure in an electric furnace (Lindberg/Blue M Mini-Mite Tube Furnace, Thermo Scientific). At this time, CH_4 (5 sccm) was introduced in the tube for 9 min to grow graphene, followed by cooling of the furnace to room temperature in a flowing Ar/H_2 atmosphere. Next, CNTs were grown on the surface of the graphene-formed Cu foil by a second CVD. To achieve this, the graphene-formed Cu foil was decorated with an Fe film 1.5 nm thick, which acts a catalyst for CNTs growth, using an e-beam evaporator (Model Temescal BJD-1800, Technical Engineering Services). The graphene/Cu foil with the Fe film was placed back in the quartz tube and heated to 750 °C in flowing Ar (100 sccm) and H_2 (50 sccm) atmosphere. After the temperature was stabilized at 750 °C, a 15 sccm flow of C_2H_2 was supplied in the tube for 5 min, followed by cooling of the furnace to room temperature in a flowing Ar/H_2 atmosphere. The CNTs/G film formed on the backside of Cu foil was removed by O_2 plasma, followed by etching of the Cu foil in a 1 M $FeCl_3$ aqueous solution to obtain the CNTs/G film. The CNTs/G film was cleaned with 5% HCl solution to completely remove the Cu foil and the Fe nanoparticles. Note that we also obtained the graphene film using the same procedure. The morphology of the CNTs/G film was observed using field-emission scanning electron microscopy (FE-SEM) (Philips, Model XL30 FEG system). The CNTs/G film was also characterized using Raman spectrometer (LabRAM HR Evolution, Horiba, Ltd.) and XPS (PHI Quantera SXM, Ulvac-Phi, Inc.).

Preparation of HP-Modified CNTs/G Hybrid Electrodes. A glassy carbon (GC) electrode (3 mm in diameter, ALS Co., Ltd.) was polished with 1 and 0.05 μm alumina slurries on a polishing cloth and then thoroughly rinsed with distilled water. The GC electrode was sonicated in 2-propanol and distilled water, respectively, and then dried with a high-purity nitrogen stream. The CNTs/G or graphene film was transferred to the GC electrode surface, followed by drying at 50 °C in an electric oven for 1 h to obtain CNTs/G and graphene electrodes (Figure 1). The CNTs/G and graphene electrodes were subsequently immersed in *N*,*N*-dimethylformamide (DMF) containing 6.0 mM 1-pyrenebutyric acid *N*-hydroxysuccinimide ester (PBASE) for 30 min. After thoroughly rinsing with DMF and 67 mM phosphate buffer (pH 7.4), the electrodes were immersed in the 67 mM phosphate buffer (pH 7.4) containing 1.0 mM HP (Sigma−Aldrich) for 12 h at 4 °C to obtain HP/CNTs/G and HP/G electrodes.

To fabricate HP-ML/CNTs/G and HP-ML/G electrodes, 12 μL of 0.1 M 2-morpholinoethanesulfonic (MES) aqueous solution (pH 4.6) containing 1 mM HP and 0.3 M 1-ethyl-3-(3-(dimethylamino)propyl) carbodiimide (EDC) was cast on the surfaces of HP/CNTs/G and HP/G electrodes. Afterward, these electrodes were stored at 4 °C for 12 h and thoroughly rinsed with distilled water to remove excess casting solution.

Electrochemical Measurements. Electrochemical measurements were performed in 67 mM phosphate buffer (pH 7.4) in a batch system. A Ag|AgCl|KCl (sat.) and a coiled platinum

DOI: 10.1021/am508032p
ACS Appl. Mater. Interfaces 2015, 7, 3647−3654

wire were used as reference and counter electrodes, respectively.

The CNTs/G electrode was evaluated in a 0.1 M KCl aqueous solution containing 1.0 mM $[Ru(NH_3)_6]Cl_3$ by cyclic voltammetry (CV) using a potentiostat (Model CHI750c, CH Instruments Inc., USA). Direct electron transfer reaction between HP and the electrode through CNTs/G or graphene film was evaluated by CV using a potentiostat (Model HSV-110, Hokuto Denko). The catalytic activity of HP/CNTs/G, HP/G, HP-ML/CNTs/G, and HP-ML/G electrodes toward H_2O_2 reduction was evaluated by amperometry with the potentiostat (Model LC-4C, BAS). After the working electrode was polarized at +150 mV and a steady-state current was obtained, a H_2O_2 solution was added into the electrolyte solution. From the steady-state current obtained, the catalytic activity of HP at the CNTs/G and graphene electrodes was determined.

RESULTS AND DISCUSSION

Characterization of CNTs/G Hybrid Films. Figure 2A shows a photograph of CNTs/G hybrid films floating on water after chemical etching of Cu foil, indicating the formation of a large area film on Cu foil. Therefore, the CNTs/G hybrid film can be transferred to flat substrates, because CNTs basically grow at the flat graphene surface. Figures 2B and 2C show FE-SEM images of the surface and cross-section of the CNTs/G hybrid film, respectively. We presume that the CNTs grew perpendicularly at the graphene surface during the early stage and then the tip of CNT fell down on neighboring CNTs during the later stage, resulting in the formation of a chain conformation and/or a network-like structure. This indicates that Fe nanoparticles formed on the graphene surface for CNTs growth were randomly distributed on the graphene surface. Such a structure will allow one to increase the surface coverage of chemicals, such as enzymes, because of the suppression of carbon nanotube bundle effects.

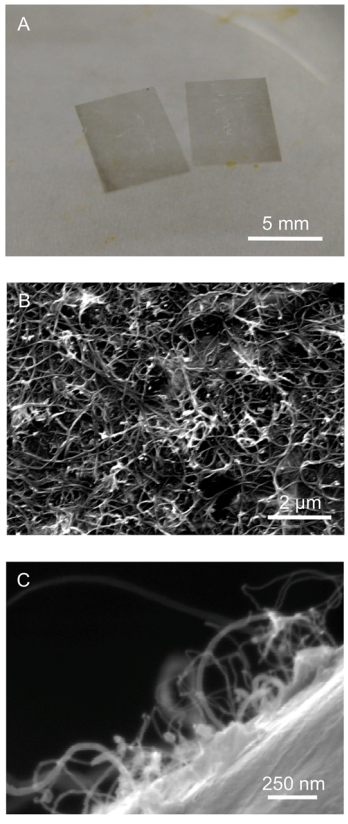

Figure 2. (A) Photograph of CNTs/G films floating on distilled water. FE-SEM images of the (B) surface and (C) cross-section of the CNTs/G film.

Figure 3A shows Raman spectra before and after growth of CNTs on graphene. sp^2 carbon atoms, such as graphene, generally give a *G* band signal at ~1580 cm^{-1} and a *G′* band signal at ~2700 cm^{-1}.[15] Meanwhile, C atoms adjacent to a defect or a graphene edge give a *D* band signal at ~1350 cm^{-1}.[16] As shown (spectrum a in Figure 3A), the *G* and *G′* bands clearly appeared at 1584 and 2678 cm^{-1}, respectively. The *G*/*G′* band intensity ratio was ~0.25. It is known that the *G* band and the *G*/*G′* ratio for monolayer graphene are ~1584 cm^{-1} and 0.25, respectively,[17] which confirms the formation of a monolayer graphene. After growth of CNTs on the graphene surface, the *D* band also appeared at ~1350 cm^{-1}, in addition to the *G* band (spectrum b in Figure 3A). The *D*/*G* band intensity ratio was calculated to be ~0.86. Unlike in the case of graphene, the *G* band intensity was much larger than that of the *G′* band. The *G′* band for the CNTs/G film was shifted 22 cm^{-1} higher than that for graphene. The *G*/*G′* band intensity ratio was estimated to be ~2.72. These results fitted the characteristics of few-layer graphene[17] and is attributed to the 3D structure consisting of multiwalled carbon nanotubes (MWCNTs) grown on the monolayer graphene.

We further characterized the CNTs/G film by XPS. In the deconvoluted C1 spectrum (Figure 3B), a main peak of the graphitic structure appeared at ~284.3 eV. Moreover, five peaks attributed to defects on the nanotube structure (ca. 285.3 eV), oxygen-containing functional groups (ca. 286.7, 288.6, and 290.3 eV), and $\pi-\pi^*$ transition (ca. 291.6 eV) were obtained.[18] In the deconvoluted O1 spectrum (Figure 3C), two peaks attributed to oxygen-containing functional groups (ca. 531.7 and 533.3 eV) were also observed.[18] Based on these spectra, the atomic oxygen/carbon (O/C) ratio of the CNTs/G film was determined to be ~12.3%. The reason that the oxygen-containing functional groups existed at the CNTs/G film might be due to the acid treatment for the removal of Cu foil and Fe nanoparticles (see the Experimental Section). In addition, the CNTs/G film might be oxidized by atmospheric oxygen. Although the peaks for defects on the nanotube structure was obtained here, there was no obvious *D′* band (ca. 1620 cm^{-1}), which is an index of the presence of graphene edges, in the Raman spectrum (see Figure 3A).[19] We supposed that the CNTs/G film was not heavily oxidized by the acid treatment.

Next, we examined electrochemical behavior of $[Ru(NH_3)_6]Cl_3$, the electron transfer kinetics of which is generally known to be an outer-sphere process and independent of surface sites and/or functional groups,[20] at the CNTs/G electrode. Figure 3D shows CVs recorded in a 0.1 M KCl aqueous solution containing 1 mM $[Ru(NH_3)_6]Cl_3$, where the scan rate was 25 mV s^{-1}. The reversible redox peak current at the CNTs/G electrode was ~2.5 times larger than that at the graphene electrode, indicating an increased apparent electroactive surface area (A_{app}), because of CNTs grown at the graphene surface. The A_{app} value for the CNTs/G film was compared with that for the graphene film, using the Randles–Sevcik equation:[21]

$$I_p = (2.69 \times 10^5) n^{3/2} A_{app} D^{1/2} C \nu^{1/2} \quad (1)$$

DOI: 10.1021/am508032p
ACS Appl. Mater. Interfaces 2015, 7, 3647–3654

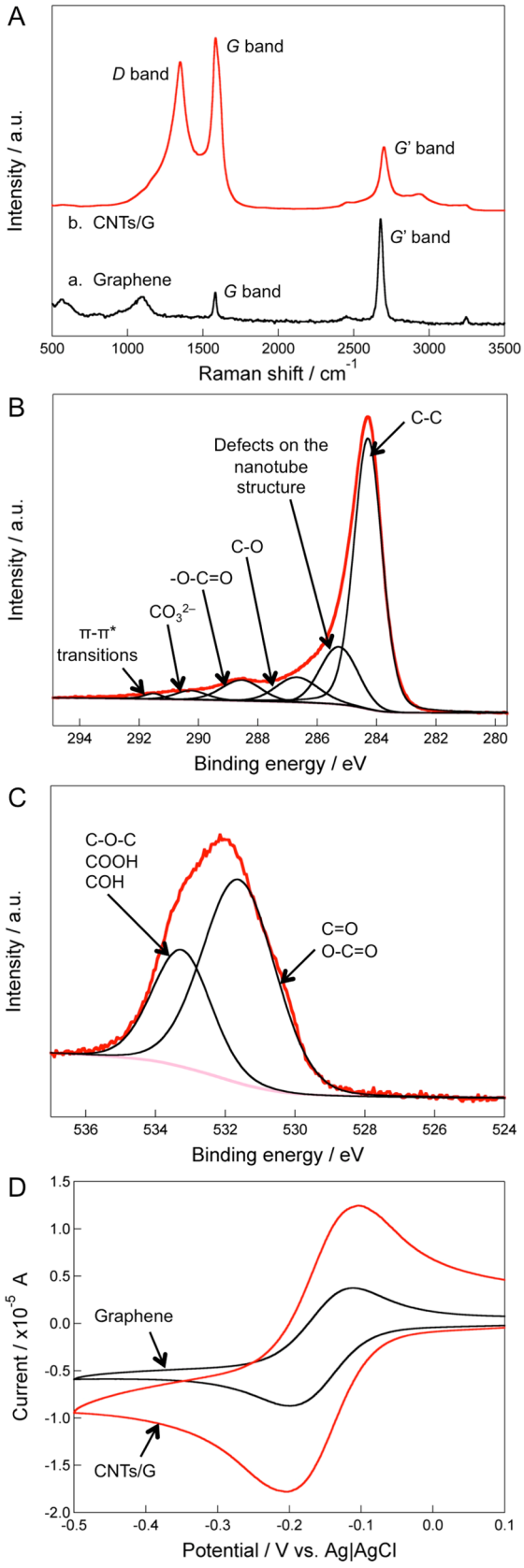

Figure 3. (A) Raman spectra of (a) graphene and (b) the CNTs/G film. XPS (B) C1 and (C) O1 spectra of the CNTs/G film. (D) CVs of 1.0 mM $[Ru(NH_3)_6]Cl_3$ in a 0.1 M KCl aqueous solution at the CNTs/G and graphene electrodes at a scan rate of 25 mV s^{-1}.

where n is the number of electrons transferred (n = 1), D the diffusion coefficient of $[Ru(NH_3)_6]^{2+/3+}$ (D = 9.1 × 10^{-6} cm^2 s^{-1}),[22] C the concentration of $[Ru(NH_3)_6]Cl^3$, and ν the scan rate. The A_{app} values for the CNTs/G and graphene films were ~0.141 and 0.059 cm^2, respectively. We further examined the stability of the CNTs/G film on the GC surface using the multiple scan CV measurement. If fragile, the CNTs/G film would be detached from the GC surface and, as a result, the redox peak current of $[Ru(NH_3)_6]^{2+/3+}$ would decrease. However, the redox peak current was approximately constant for at least 20 repeated cyclic potential sweeps, from −0.5 V to 0.1 V, at a scan rate of 100 mV s^{-1} (see Figure S1 in the Supporting Information), confirming that the CNTs/G film was tightly attached at the GC surface, because of $\pi-\pi$ and/or hydrophobic interactions.

Electrochemical Characterization of HP-Modified CNTs/G Hybrid Electrodes. CV measurements were carried out with the HP/G and HP/CNTs/G electrodes in 67 mM phosphate buffer (pH 7.4). As shown in Figure 4A, reversible redox peaks appeared at approximately −370 mV (vs Ag|AgCl) in HP/G and HP/CNTs/G electrodes, corresponding to $(P)Fe^{2+/3+}$ (P = porphyrin ring),[23,24] whereas no redox peak was observed without HP (Figure 4B). The redox peak currents per the GC surface area (ca. 7.1 × 10^{-2} cm^2) at the HP/CNTs/G electrode were about 1 order of magnitude larger than those at the HP/G. Since the peak currents for both electrodes were proportional to the scan rate below at least 100 mV s^{-1} (Figure 4C), the redox peak currents were used to estimate the surface coverage Γ of electroactive HP at the CNTs/G film and graphene, using the equation

$$i_p = \frac{n^2F^2\Gamma\nu}{4RT} \quad (2)$$

where n is the number of electrons transferred (n = 1), F the Faraday constant, R the gas constant, and T the temperature. Based on the equation, the Γ values were estimated to be 1.3 × 10^{-11} and 1.1 × 10^{-10} mol cm^{-2} for the graphene (i_p/ν = 1.2 × 10^{-5} A cm^{-2} V^{-1} s) and CNTs/G electrodes (i_p/ν = 1.0 × 10^{-4} A cm^{-2} V^{-1} s), respectively. The one-order-of-magnitude-higher value of the coverage for the CNTs/G is attributed to the larger electroactive surface area, as a result of the 3D structure. Furthermore, based on the reported Γ value for the HP monolayer-modified gold electrode (3.5 × 10^{-11} mol cm^{-2}), we hypothesize that there was a monolayer coverage of HP at both graphene and CNTs/G electrodes.[25]

Catalytic Reduction of H_2O_2. Cathodic current responses of the HP/CNTs/G electrode to H_2O_2 were measured at +150 mV (vs Ag|AgCl) in an air-saturated 67 mM phosphate buffer solution (pH 7.4). After the background current stabilized, aliquots of H_2O_2 were added to the electrolyte solution and a steady-state cathodic current was observed after each addition. This current is attributed to electron transfer from the electrode to HP via the CNTs/G hybrid film. The possible reaction mechanisms are

$$\text{ferric HP} + H_2O_2 \rightarrow \text{compound I} + H_2O \quad (3)$$

$$\text{compound I} + e^- + H^+ \rightarrow \text{compound II} \quad (4)$$

$$\text{compound II} + e^- + H^+ \rightarrow \text{ferric HP} + H_2O \quad (5)$$

where compound I and II are oxidized complexes of HP, in which the Fe(IV) of heme is coordinated to oxygen.[12,13] As shown in Figure 5A, the steady-state cathodic current densities

DOI: 10.1021/am508032p
ACS Appl. Mater. Interfaces 2015, 7, 3647−3654

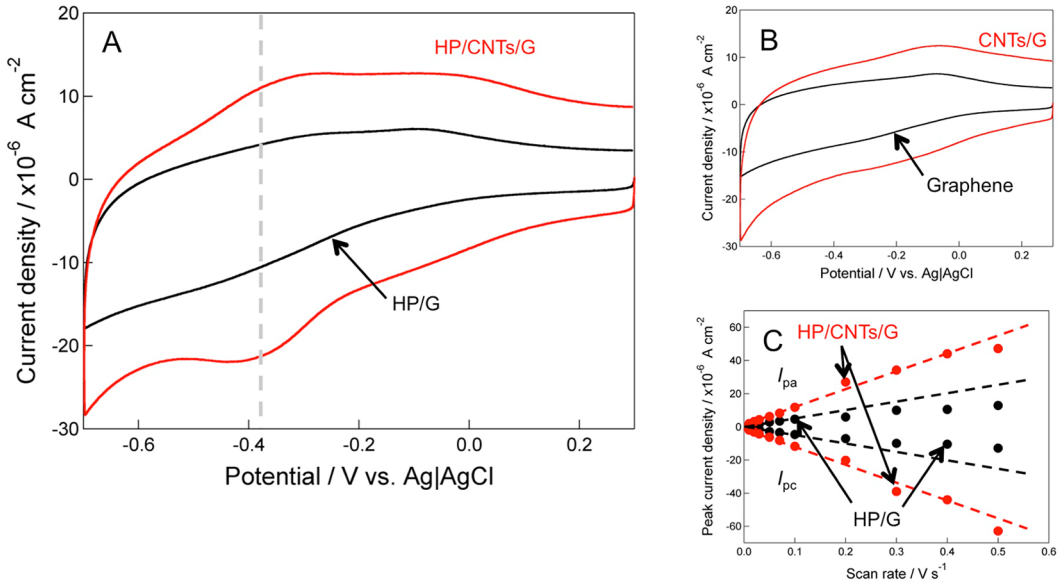

Figure 4. CVs of (A) HP/CNTs/G and HP/G and (B) CNTs/G and graphene electrodes in a 67 mM phosphate buffer solution (pH 7.4) at scan rate of 100 mV s^{-1}. (C) Relationship between anodic and cathodic peak currents of HP/CNTs/G and HP/G electrodes and scan rate.

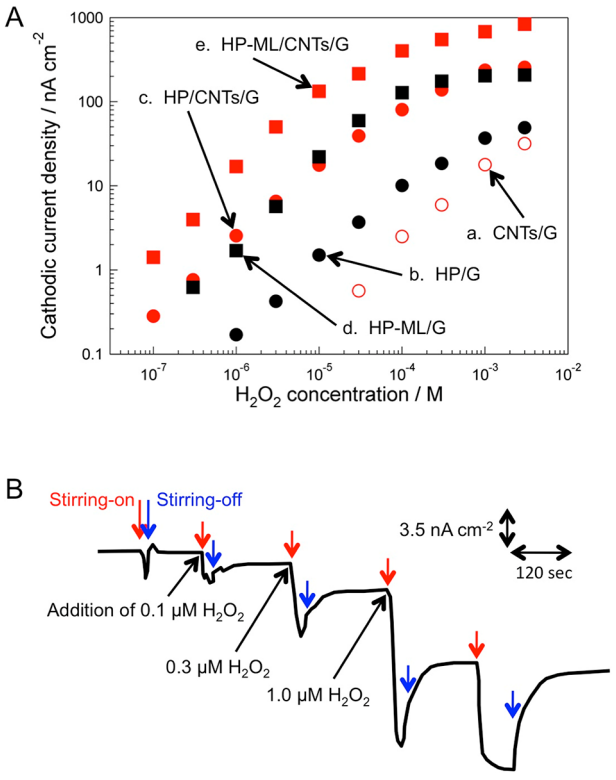

Figure 5. (A) Cathodic current densities of H_2O_2 reduction at the CNTs/G electrode (plot a), the HP/G electrode ($\Gamma = 1.3 \times 10^{-11}$ mol cm^{-2}) (plot b), the HP/CNTs/G electrode ($\Gamma = 1.1 \times 10^{-10}$ mol cm^{-2}) (plot c), the HP-ML/G ($\Gamma = 5.5 \times 10^{-10}$ mol cm^{-2}) (plot d), and the HP-ML/CNTs/G ($\Gamma = 5.5 \times 10^{-10}$ mol cm^{-2}) electrode (plot e). (B) Chronoamperometric response of the HP-ML/CNTs/G electrode to H_2O_2 in an air-saturated 67 mM phosphate buffer solution (pH 7.4) at +150 mV vs Ag|AgCl.

for H_2O_2 reduction at the HP/CNTs/G electrode were clearly much larger than those at the bare CNTs/G electrodes. In addition, the cathodic currents at the HP/CNTs/G electrode were larger than those at the HP/G electrode. The cathodic current at the HP/CNTs/G and HP/G electrodes linearly increased for H_2O_2 concentration between 0.1×10^{-6} and 3.0×10^{-5} M, indicating that eq 3 was the rate-determining step of the reaction. However, for H_2O_2 concentrations of 3.0×10^{-4} M or higher, the cathodic current was independent of the H_2O_2 concentration, indicating that eq 4 and/or 5 were the rate-determining steps. In addition, the catalytic cathodic currents obtained at both HP/CNTs/G and HP/G electrodes were found to be kinetically controlled, because the current response was not influenced when the electrolyte solution was stirred.

The kinetics of the reactions were analyzed on the basis of the observed currents (Figure 5A) and the HP coverage. As mentioned above, since the catalytic cathodic current for H_2O_2 reduction was kinetically controlled, all the HP molecules should contribute to the current and the current should be proportional to the surface coverage of HP. Therefore, the cathodic current i is given by eq 6.[12,13,26,27]

$$i = \frac{2F\Gamma}{\left(\frac{1}{k_1 C_S} + \frac{k_2 + k_3}{k_2 k_3 C_H}\right)} \quad (6)$$

where k_1, k_2, and k_3 are the rate constant of eqs 3–5, and C_S and C_H are the H_2O_2 and proton concentration in the bulk solution, respectively. According to eq 6, based on the Γ the catalytic current at the HP/CNTs/G electrode should be approximately an order of magnitude larger than at the HP/G electrode. This was indeed observed experimentally (Figure 5A).

Using eq 6, we calculated the rate constants for the three reactions. In the linear response region ($[H_2O_2] \leq 3.0 \times 10^{-5}$ M), the current response is determined by the rate of eq 3. Since eq 3 is kinetically controlled, the current is given by the equation

$$i_1 = 2F\Gamma k_1 C_S \quad (7)$$

The k_1 values were estimated from eq 7 to be ~120 M^{-1} s^{-1} for the HP/CNTs/G electrode ($i/C_S = 2.5 \times 10^{-3}$ A cm^{-2} M^{-1} at 0.1×10^{-6} to 1.0×10^{-6} M H_2O_2) and 40 M^{-1} s^{-1} for the HP/G electrode ($i/C_S = 1.0 \times 10^{-4}$ A cm^{-2} M^{-1} at 1.0×10^{-6} to 1.0×10^{-5} M H_2O_2), respectively. It is known that the k_1

DOI: 10.1021/am508032p
ACS Appl. Mater. Interfaces 2015, 7, 3647–3654

value at a heme nonapeptide-modified SnO_2-coated glass plate was 220 M^{-1} s^{-1}[112] and was much smaller than those obtained for HRP-adsorbed graphite electrode by Ruzgas et al. (3.9×10^4 M^{-1} s^{-1})[28] and Tatsuma et al. (3.1×10^4 M^{-1} s^{-1}),[29] because of the difference in molecular complexity. We believe that the same tendency was observed in our present work. In the constant region ($\geq 3.0 \times 10^{-4}$ M), the current response is determined by the rates of eqs 4 and 5. If those equations are not controlled by the diffusion of protons but instead by the enzymatic reactions, including electron transfer from CNTs/G or graphene to compound I and II, the current is given by the equation

$$i_{23} = \frac{2F\Gamma k_2 k_3 C_H}{k_2 + k_3} \quad (8)$$

Substituting the i_{23} values of 2.6×10^{-7} or 4.9×10^{-8} A cm^{-2} at 3.0×10^{-3} M H_2O_2 for the HP/CNTs/G or HP/G electrodes (see Figure 5A), respectively, the C_H value ($\sim 4.0 \times 10^{-8}$ M), F, and Γ ($\Gamma = 1.1 \times 10^{-10}$ mol cm^{-2} for the HP/CNTs/G electrode or 1.3×10^{-11} mol cm^{-2} for the HP/G electrode) into eq 8, the $k_2k_3/(k_2 + k_3)$ value was calculated to be $\sim 3.0 \times 10^5$ and 4.9×10^5 M^{-1} s^{-1} at the HP/CNTs/G and HP/G electrodes, respectively. The $k_2k_3/(k_2 + k_3)$ value at the HP/CNTs/G electrode is slightly smaller than that at the HP/G one. This might be comparably reasonable, because the CNTs/G film consisted of the multilayered graphene. The $k_2k_3/(k_2 + k_3)$ values obtained here were one order of magnitude smaller than that obtained at pH 7.0 for the HRP-adsorbed graphite electrode by Ruzgas et al. (6.6×10^6 M^{-1} s^{-1}),[28] although the molecular weight of HP is 1 order of magnitude smaller than that of HRP. This is presumably affected by the difference in the plane site of carbon nanotmaterials. It has been known that the heterogeneous electron transfer rate constant at the edge plane site of graphite was ~6 orders of magnitude larger than that at the basal plane.[30] Therefore, such a decline in the $k_2k_3/(k_2 + k_3)$ value was likely due to the fact that HRP was adsorbed at the edge plane site of graphite, whereas HP was immobilized at the basal plane of CNTs.

We initially expected to obtain the same k_1 value at the HP/CNTs/G and HP/G electrodes, because HP molecules were just immobilized on the basal plane of the sp^2 bonded C atoms via PBASE. However, the k_1 value at the HP/CNTs/G electrode was ~3 times larger than that at the HP/G electrode. The reason for this is unclear; however, it is presumable that the chain conformation and/or network-like structure of CNTs/G at the graphene surface is involved in the acceleration of eq 3. Compared with the 2D graphene surface, CNTs modified with HP molecules might easily sway back and forth and around. In addition, $\pi-\pi$ interaction among CNTs might stabilize HP molecules. Therefore, based on these, the k_1 value at the HP/CNTs/G electrode might increase, in comparison with that at the HP/G electrode. On the other hand, we also suspect the involvement of defects in CNTs for such enhancement of the k_1 value, because the D band appeared at the CNTs/G film but not graphene (Figure 3A). If the defects of CNTs are involved in the stabilization of HP, the $k_2k_3/(k_2 + k_3)$ value at the HP/CNTs/G electrode should be much larger than that at the HP/G electrode, because the defects of CNTs work as the edge plane sites. However, as mentioned above, the $k_2k_3/(k_2 + k_3)$ value at the HP/CNTs/G electrode was slightly smaller than that at the HP/G electrode. In the present work, the defects of CNTs had little effect on k_1.

We also calculated the apparent Michaelis–Menten constant (K_M^{app}). From eq 6 and the Michaelis–Menten kinetics equation ($i = i_{23}C_S/(K_M^{app} + C_S)$), K_M^{app} is given by the following equation:

$$K_M^{app} = \frac{k_2 k_3 C_H}{k_1(k_2 + k_3)} \quad (9)$$

As a result, the K_M^{app} values at the HP/CNTs/G and HP/G electrodes were determined to be $\sim 1.0 \times 10^{-4}$ and $\sim 3.0 \times 10^{-4}$ M, respectively. These values were at least 1 order of magnitude lower than that obtained at a polymerized carbon electrode containing HP by Razumas et al. (6.4×10^{-3} M, pH 7.0).[31] Since the K_M^{app} value at the HP/CNTs/G electrode was lower than that at the HP/G electrode, the CNTs/G film could be therefore useful as a conductive nanoscaffold for enzymes to develop highly sensitive enzyme-based electrochemical biosensors.

Effect of Microvoids in CNTs/G Hybrid Films. We further examined diffusion benefits of the microvoid within CNTs/G hybrid films (see Figures 2B and 2C) for H_2O_2 and/or H^+ on electrochemical responses. If the CNTs/G film and graphene are excessively immobilized with the same amounts of HP molecules and diffusion of H_2O_2 and/or H^+ is not influenced by the microvoid in the CNTs/G film, the cathodic current should show roughly the same values, because of the self-mediation among HP molecules.[13] In order to demonstrate the issue, we used the HP-ML/CNTs/G and HP-ML/G electrodes, the Γ values of which were determined to be $\sim 5.5 \times 10^{-10}$ mol cm^{-2} from the integration of CV peaks (charge) at the scan rate of 10 mV s^{-1} (see Figure S2 in the Supporting Information). As shown in Figure 4, the cathodic currents at the HP-ML/CNTs/G and HP-ML/G electrodes were larger than those at the HP/CNTs/G and HP/G electrodes, respectively, because of the increase in the Γ value. However, the cathodic current at the HP-ML/CNTs/G electrode was 5–7 times larger than that at the HP-ML/G electrode. This difference is likely due to the contribution of microvoids in the CNTs/G film.

In the HP-ML/G electrode, the Γ value increased by a factor of ~26, compared to that at the HP/G electrode, but the cathodic current increased by a factor of only ~10. This is because the rate-determining step for the HP-ML/G electrode is the diffusion of H_2O_2 ($\leq 3.0 \times 10^{-5}$ M) or proton and/or e^- of the electron self-exchange ($\geq 3.0 \times 10^{-5}$ M), as previously reported.[13] In fact, the catalytic current for H_2O_2 reduction at the HP-ML/G electrode significantly increased when the electrolyte solution was stirred. The HP molecules at only the interface of the HP-ML/G electrode might partially contribute to the H_2O_2 reduction, because of their dense and tight immobilization on the flat surface of graphene. This means that the cathodic current does not increase, even if the Γ value increases. In contrast, the cathodic current at the HP-ML/CNTs/G electrode was 5–7 times larger than that at the HP/CNTs/G electrode. Also, the catalytic current for the H_2O_2 reduction at the HP-ML/CNTs/G electrode slightly increased when the electrolyte solution was stirred, which indicates that the rate-determining step for the HP-ML/CNTs/G electrode might also be the diffusion of H_2O_2 or proton and/or e^- of the electron self-exchange (Figure 5B). However, the cathodic current at the HP-ML/CNTs/G electrode was larger than that at the HP-ML/G electrode, as described above. In addition, the cathodic current at the HP-ML/CNTs/G electrode was 15–17 times greater than that at the HP/G

DOI: 10.1021/am508032p
ACS Appl. Mater. Interfaces 2015, 7, 3647–3654

electrode. Thus, the microvoids in the CNTs/G film helps the diffusion of H_2O_2 and/or proton to HP molecules. We can therefore conclude that, compared with the graphene electrode, the sensitivity is significantly enhanced at the CNTs/G electrode, because of the increase in the surface coverage of enzymes and the effect of the microvoids for diffusion of substrates. Further investigation of the selectivity to analytes and interference with biological molecules will have to be assessed for the development of a practical biosensor for H_2O_2 in a human body. In addition, this work would be expected to lead to the development of not only enzyme-based highly sensitive electrochemical biosensors but also enzyme-based biofuel cells.

CONCLUSION

The CNTs/G film was formed by two-step CVD process. CNTs were randomly and loosely grown at the graphene monolayer, resulting in the presence of microvoids. We constructed the highly sensitive electrochemical biosensor for H_2O_2 using the CNTs/G film as the conductive nanoscaffolds for HP molecules. Compared with the HP/G electrode, the catalytic current for H_2O_2 reduction at the HP-ML/CNTs/G electrode increased by a factor of ~15. In addition, microvoids in the CNTs/G film played a significant role in the diffusion of H_2O_2 into modified HP. The CNTs/G film would be useful not only for electrochemical biosensors but also for enzyme-based biofuel cells.

ASSOCIATED CONTENT

Supporting Information

Multiple CVs of $[Ru(NH_3)_6]^{2+/3+}$ at the CNTs/G electrode; CVs of HP-ML/CNTs/G and HP-ML/G electrodes. This material is available free of charge via the Internet at http://pubs.acs.org.

AUTHOR INFORMATION

Corresponding Authors

*E-mail: kkomori@iis.u-tokyo.ac.jp (K. Komori).
*E-mail: adani@engr.ucr.edu (A. Mulchandani).

Notes

The authors declare no competing financial interest.

ACKNOWLEDGMENTS

We are very grateful to Dr. T. Sarkar for valuable discussions, Dr. M. Kamiko for his help with the XPS measurements, and Ms. T. Numata for her help with the Raman spectroscopic measurements. This work was partially supported by a Young Researchers Overseas Study Program for Mechanical System Innovation of University of Tokyo, Japan (for K.K.) and a Grant-in-Aid for Young Scientist (B) (No. 26790011 for K.K.) from the Ministry of Education, Culture, Sports, Science, and Technology (MEXT), Japan. A.M. is grateful for support from the W. Ruel Johnson Chair in Environmental Engineering and USDA grant 2014-67021-21589.

REFERENCES

(1) Baughman, R. H.; Zakhidov, A. A.; de Heer, W. A. Carbon Nanotubes—The Route Toward Applications. *Science* **2002**, *297*, 787−792.
(2) Novoselov, K. S.; Fal'ko, V. I.; Colombo, L.; Gellert, P. R.; Schwab, M. G.; Kim, K. A Roadmap for Graphene. *Nature* **2012**, *490*, 192−200.
(3) De Volder, M. F. L.; Tawfick, S. H.; Baughman, R. H.; Hart, A. J. Carbon Nanotubes: Present and Future Commercial Applications. *Science* **2013**, *339*, 535−539.
(4) Cai, C.; Chen, J. Direct Electron Transfer of Glucose Oxidase Promoted by Carbon Nanotubes. *Anal. Biochem.* **2004**, *332*, 75−83.
(5) Yan, Y.; Zheng, W.; Zhang, M.; Wang, L.; Su, L.; Mao, L. Bioelectrochemically Functional Nanohybrids through Co-Assembling of Proteins and Surfactants onto Carbon Nanotubes: Facilitated Electron Transfer of Assembled Proteins with Enhanced Faradic Response. *Langmuir* **2005**, *21*, 6560−6566.
(6) Kang, X.; Wang, J.; Wu, H.; Aksay, I. A.; Liu, J.; Lin, Y. Glucose Oxidase−Graphene−Chitosan Modified Electrode for Direct Electrochemistry and Glucose Sensing. *Biosens. Bioelectron.* **2009**, *25*, 901−905.
(7) Zhang, Q.; Qiao, Y.; Hao, F.; Zhang, L.; Wu, S.; Li, Y.; Li, J.; Song, X.-M. Fabrication of a Biocompatible and Conductive Platform Based on a Single-Strand DNA/Graphene Nanocomposite for Direct Electrochemistry and Electrocatalysis. *Chem.—Eur. J.* **2010**, *16*, 8133−8139.
(8) Chen, Z.; Ren, W.; Gao, L.; Liu, B.; Pei, S.; Cheng, H.-M. Three-Dimensional Flexible and Conductive Interconnected Graphene Networks Grown by Chemical Vapor Deposition. *Nat. Mater.* **2011**, *10*, 424−428.
(9) Wang, X.; Zhang, Y.; Zhi, C.; Wang, X.; Tang, Z.; Xu, Y.; Weng, Q.; Jiang, X.; Mitome, M.; Golberg, D.; Bando, Y. Three-Dimensional Strutted Graphene Grown by Substrate-Free Suger Blowing for High-Power-Density Supercapacitors. *Nat. Commun.* **2013**, *4*, 2905.
(10) Paul, R. K.; Ghazinejad, M.; Penchev, M.; Lin, J.; Ozkan, M.; Ozkan, C. S. Synthesis of a Pillared Graphene Nanostructure: A Counterpart of Three-Dimensional Carbon Architectures. *Small* **2010**, *6*, 2309−2313.
(11) Zhu, Y.; Li, L.; Zhang, C.; Casillas, G.; Sun, Z.; Yan, Z.; Ruan, G.; Peng, Z.; Raji, A.-R. O.; Kittrell, C.; Hauge, R. H.; Tour, J. M. A Seamless Three-Dimensional Carbon Nanotube Graphene Hybrid Material. *Nat. Commun.* **2012**, *3*, 1225.
(12) Tatsuma, T.; Watanabe, T. Peroxidase Model Electrodes: Heme Peptide Modified Electrodes as Reagentless Sensors for Hydrogen Peroxide. *Anal. Chem.* **1991**, *63*, 1580−1585.
(13) Komori, K.; Takada, K.; Tatsuma, T. Peroxidase Model Electrodes: Self-Mediation of Heme Peptide Multilayer-Modified Electrodes and its Application to Biosensing with Adjustable Dynamic Range. *J. Electroanal. Chem.* **2005**, *585*, 89−96.
(14) Komori, K.; Takada, K.; Tatsuma, T. Electrodes Modified with Phase Transition Polymer and Heme Peptide: Biocatalysis and Biosensing with Tunable Activity and Dynamic Range. *Langmuir* **2006**, *22*, 478−483.
(15) Ferrari, A. C.; Meyer, J. C.; Scardaci, V.; Casiraghi, C.; Lazzeri, M.; Mauri, F.; Piscanec, S.; Jiang, D.; Novoselov, K. S.; Roth, S.; Geim, A. K. Raman Spectrum of Graphene and Graphene Layer. *Phys. Rev. Lett.* **2006**, *97*, 187401.
(16) Dresselhaus, M. S.; Jorio, A.; Hofmann, M.; Dresselhaus, G.; Saito, R. Perspectives on Carbon Nanotubes and Graphene Raman Spectroscopy. *Nano Lett.* **2010**, *10*, 751−758.
(17) Graf, D.; Molitor, F.; Ensslin, K.; Stampfer, C.; Jungen, A.; Hierold, C.; Wirtz, L. Spatially Resolved Raman Spectroscopy of Single- and Few-Layer Graphene. *Nano Lett.* **2007**, *7*, 238−242.
(18) Datsyuk, V.; Kalyva, M.; Papagelis, K.; Parthenios, J.; Tasis, D.; Siokou, A.; Kallitsis, I.; Galiotis, C. Chemical Oxidation of Multiwalled Carbon Nanotubes. *Carbon* **2008**, *46*, 833−840.
(19) Jang, I. Y.; Ogata, H.; Park, K. C.; Lee, S. H.; Park, J. S.; Jung, Y. C.; Kim, Y. J.; Kim, Y. A.; Endo, M. Exposed Edge Planes of Cup-Stacked Carbon Nanotubes for an Electrochemical Capacitor. *J. Phys. Chem. Lett.* **2010**, *1*, 2099−2103.
(20) Chen, P.; McCreery, R. L. Control of Electron Transfer Kinetics at Glassy Carbon Electrodes by Specific Surface Modification. *Anal. Chem.* **1996**, *68*, 3958−3965.
(21) Bard, A. J.; Faukner, L. R. *Electrochemical Methods: Fundamentals and Applications*, 2nd Edition; John Wiley & Sons: New York, 2001.

DOI: 10.1021/am508032p
ACS Appl. Mater. Interfaces 2015, 7, 3647−3654

(22) Marken, F.; Eklund, J. C.; Compton, R. G. Voltammetry in the Presence of Ultrasound: Can Ultrasound Modify Heterogeneous Electron Transfer Kinetics? *J. Electroanal. Chem.* **1995**, *395*, 335−339.
(23) Razumas, V.; Kazlauskaite, J.; Ruzgas, T.; Kulys, J. Bioelectrochemistry of Microperoxidases. *Bioelectrochem. Bioenerg.* **1992**, *28*, 159−176.
(24) Ruzgas, T.; Gaigalas, T.; Gorton, L. Diffusionless Electron Transfer of Microperoxidase-11 on Gold Electrode. *J. Electroanal. Chem.* **1999**, *469*, 123−131.
(25) Gooding, J. J.; Wibowo, R.; Liu, J.; Yang, W.; Losic, D.; Orbons, S.; Mearns, S. J.; Shapter, J. G.; Hibbert, D. B. Protein Electrochemistry Using Aligned Carbon Nanotube Arrays. *J. Am. Chem. Soc.* **2003**, *125*, 9006−9007.
(26) Tatsuma, T.; Watanabe, T. Model Analysis of Enzyme Monolayer- and Bilayer-Modified Electrodes: The Steady-State Response. *Anal. Chem.* **1992**, *64*, 625−630.
(27) Ko, S.; Takahashi, Y.; Fujita, H.; Tatsuma, T.; Sakoda, A.; Komori, K. Peroxidase-Modified Cup-Stacked Carbon Nanofiber Networks for Electrochemical Biosensing with Adjustable Dynamic Range. *RSC Adv.* **2012**, *2*, 1444−1449.
(28) Ruzgas, T.; Gorton, L.; Emnéus, J.; Marko-Varga, G. Kinetic Models of Horseradish Peroxidase Action on a Graphite Electrode. *J. Electroanal. Chem.* **1995**, *391*, 41−49.
(29) Tatsuma, T.; Ariyama, K.; Oyama, N. Kinetic Analysis of Electron Transfer From a Graphite Coating to Horseradish Peroxidase. *J. Electroanal. Chem.* **1998**, *446*, 205−209.
(30) Rice, R. J.; McCreery, R. L. Quantitative Relationship Between Electron Transfer Rate and Surface Microstructure of Laser-Modified Graphite Electrodes. *Anal. Chem.* **1989**, *61*, 1637−1641.
(31) Razumas, V.; Kazlauskaite, J.; Vidziunaite, R. Electrocatalytic Reduction of Hydrogen Peroxide on the Microperoxidase-11 Modified Carbon Paste and Graphite Electrodes. *Bioelectrochem. Bioenerg.* **1996**, *39*, 139−143.

DOI: 10.1021/am508032p
ACS Appl. Mater. Interfaces 2015, 7, 3647−3654